Hydraulics Research
Wallingford

# MEASUREMENT OF VELOCITY AND SUSPENDED SOLIDS IN AN ESTUARY

Dr H O Anwar

Report No SR 167
March 1988

Registered Office: Hydraulics Research Limited,
Wallingford, Oxfordshire OX10 8BA.
Telephone: 0491 35381. Telex: 848552

## ACKNOWLEDGEMENTS

The study reported here was carried out under Contract PECD 7/6/56 funded by the Department of the Environment. The DOE nominated officer was Dr R P Thorogood. The work was carried out by Dr H O Anwar in the Tidal Engineering Department of Hydraulics Research, Wallingford, under the management of Mr M F C Thorn. It is published on behalf of the Department of the Environment but any opinions expressed in this report are not necessarily those of the funding Department. The author wishes to express his thanks to his colleagues Mr C B Waters and those in Field Services for carrying out field measurements, and to Mr R Atkins for the data analysis.

ABSTRACT

Field measurements were made at a vertical section near the centre of the River Taw estuary over a 12 hour period during a spring tide. Mean velocity profiles were measured within 1.40m from the bed. Instantaneous mean velocity components in the horizontal and vertical direction and instantaneous concentration of suspended solids with a median particle diameter in the order of 0.04mm were measured near the bed and at 0.95m and 1.40m above the bed, at which were also measured the mean concentration of suspended solids in the particle size ranging between 0.04mm to 0.25mm. Mean velocity profiles were logarithmic, and the friction velocity agreed well with the near bed Reynolds shear stress in the peak region. The Reynolds shear stress was higher than the friction velocity in the accelerating and decelerating phases of the current.

Suspended solids in the particle size of 0.04mm were distributed uniformly throughout the depth, but the mean concentration of coarser sand decreased with increasing distance from the bed. The mean concentration of coarser suspended solids, its horizontal flux and the turbulent kinetic energy reveal hysteresis in relation with the mean velocity. No hysteresis effect was obtained between the Reynolds shear stress and the turbulent kinetic energy, indicating the applicability of the turbulent kinetic energy numerical simulation.

In practice the results of the study presented here can be used to calculate the velocity profile, bed shear stress and suspended solids flux in the peak region of an estuarine flow. They can thus be used in numerical models, using the one-dimensional energy equation given in Appendix A, to compute the flow parameters and the suspended solids flux in the accelerating and decelerating phases of a tidal current. In this way they are directly applicable to engineering studies of sediment movement, affecting flood discharge capacity or navigation, in sandy tidal channels.

CONTENTS

CONTENTS (CONT'D)

# 1 INTRODUCTION

In recent years numerical models have been widely used to calculate the transport of sediment and pollutant in estuaries. These models can produce reasonable agreement with most measured data, when empirical coefficients are suitably chosen, but the results are very sensitive to the choice of these coefficients. This indicates that a better understanding of the structure of unsteady flows is required in order to improve any predictions which may be attempted for cases in which there is limited field data (Refs 1 to 3).

When the turbulence in a boundary layer flow is subject to the time variation of the mean flow, it was shown (Refs 4 and 5) that the relationships between the mean flow parameters and the turbulent parameters, varying across the flow, is time-dependent. In other words, the response of turbulence to the temporal variation of the mean flow varies with time, and it was shown (Refs 4 and 5) that this response is not the same in the accelerating and decelerating phases of the tidal current, hence the occurrence of hysteresis.

It can be assumed in a numerical model that there is some form of similarity arguments by the fact that the turbulence and the mean flow parameters depend on instantaneous parameters, not on the history of the flow, so that the friction velocity, $U_*$, and the roughness height, $z_o$, can be used as normalized quantities to specify the flow. This similarity concept, which leads to the quasi-steady flow state of a tidal current, is only justified, when phase shifts between the mean flow parameters and the turbulent parameters are not only small, but also remain practically unchanged across the flow. This can, of course, be verified by measuring the mean flow parameters and the turbulent parameters, namely the turbulent kinetic energy and the Reynolds stresses, throughout the tidal flow. With this in mind a series of field measurements have been carried out at a vertical section near the centreline of the River Taw (see Fig 1). The river was carrying sand in suspension, and measurements were made during two full spring tidal periods. From the measured data parameters of the mean flow, the turbulence, and the suspended sediment, were determined together with the variation of salinity.

The objective of the study presented here is to determine the terms required for the development of turbulence closure models in the presence of suspended sediment, and also to examine the applicability of the turbulent kinetic energy closure model (see Appendix A) developed by Bradshaw et al (Ref 7) when the flow parameters do not obey a similarity concept. Moreover, it is hoped that the results presented here will give a better understanding of the complex flow structure of estuarine currents.

## 2 EXPERIMENTAL SITE

The estuary of the River Taw is located in southwest England and discharges to the Bristol Channel (see Fig 1). The estuary bed is fine sand with a median diameter of about 0.20mm, and becomes actively in motion during a spring tidal current; slightly finer sand was brought up into suspension. Small quantities of silt and clay, about 50mg/l, not sufficient to cause any flocculation, were also suspended, which may have slightly increased the mean density of the current. The measurements were carried out near the centreline of a section at the eastern end of the power station jetty (see Fig 2).

## 3 EQUIPMENT

A streamlined mast, supporting five Colnbrook Electromagnetic current meters (ECM) and five Braystoke current meters, was attached to the front of an "A" shaped bed-frame, which was fitted with a vertical vane to ensure that the frame aligned with the flow (see Fig 3). The mast was free to slide vertically in the frame to ensure that a circular base plate at its foot was resting on the bed. A pitch and roll sensor was also mounted on the bed-frame to monitor the orientation of the frame relative to the bed. The ECM heads were annular in design with an overall diameter of 25mm, their output representing a mean velocity within a spatial averaging width of 20mm.

These sensors were fixed at heights 0.125m, 0.35m, 0.65m, 0.95m and 1.40m measured from the circular base plate. In addition three infra-red suspended solids monitoring heads, adjacent to three pumped sample nozzles, were fixed to the mast at elevations of 0.125m, 0.35m and 0.95m. Braystoke current meters and pumped sample nozzles were also used to give field calibrations for the ECMs and infra-red heads.

Signals from the ECM heads and infra-red suspended solids heads were recorded continuously on a 14 channel FM tape recorder. A UV chart recorder was used to ensure that sensors were not picking up extraneous noise. A multi-channel digital counter was employed to register the revolutions of the Braystoke current meters and the pitch and roll sensor over a 450s period.

Pumped samples were taken at 10 to 20 minute intervals at the measuring point; about 15 litres were passed through a 40 μm filter on each occasion for suspended solids analysis.

On the other side of the measuring vessel salinity and temperature profiles were measured throughout the depth at 30 minutes intervals using a roving unit "Severn" unit. This unit comprises a salinity/temperature bridge; the resolution of salinity and temperature were ± 0.1 (ppt) and ± 0.1°C respectively.

The analogue signals from the EMC heads and infra-red suspended solids heads were passed through Chebyshev low-pass filters set at a cut-off frequency of 10 Hz. The signals were then digitized at 25 Hz, using an Intercole Spectra 11 data logging system, programmed in FORTRAN.

In an estuary the mean flow changes its direction in each cycle, and the flow may veer around the bed features as the tide rises (Ref 8). The veering flow is slow, with fluctuations much smaller than that of turbulence, hence the averaging periods of the fluctuating signals obtained from sensors should be short enough to exclude the veering effect, but sufficiently long to contain the contribution of all turbulent eddies. With this in mind continuous signals of one accelerating phase of the current were divided into a sequence of records of 5, 10 and 15 minutes durations, and from each record a linear trend was removed. It is to be noted that the trend may not be linear when the duration is long. Various parameters were then calculated for these three record lengths and the results are given in Table 1. It shows that the mean velocity $U_m$ remains almost independent of the record length, but the rms value in the mean flow direction, $(\overline{u^2})^{\frac{1}{2}}$, the vertical direction $(\overline{w^2})^{\frac{1}{2}}$ and the Reynolds stress $\overline{uw}$ increase with increasing record length. By examining the $U_m$ - variations throughout the cycle it was found that the mean velocity, $U_m$, did not vary linearly with time for the record length longer than 5 minutes. In view of this, and the possible veering effect, 5 minutes record lengths were used for all analyses.

The data analysis revealed that the EMC heads produced spurious data during the flood tide of the 7 June, and also at elevations 0.125m and 0.65m during the other tidal periods, hence these data were not included in the final analyses.

## 4 RESULTS

### 4.1 Velocity profiles

The velocity profile in a steady two-dimensional shear flow of clear water over a hydraulically rough bed obeys a logarithmic profile of the following form within an elevation z ≈ 0.25D (Ref 10), D being the boundary layer thickness:

$$\frac{U}{U_*} = \frac{1}{k} \ln \frac{z}{z_o} \qquad (1)$$

Where U is the mean velocity at elevation z, measured from the base-plate (see Fig 3), and $U_* = (\tau_o/\rho)^{\frac{1}{2}}$ is the friction velocity, $\tau_o$ being the bed shear and $\rho$ the mass density of water. In Eq (1) $z_o$ is a roughness height indicating the bed texture, and k is the Karman constant equal to 0.4. In a steady boundary layer shear flow with suspended solids it was suggested (Refs 11 and 12) that in the bed region, ($z \ll 0.1D$) k remains constant equal to 0.4, and in the upper region ($z \gg 0.1D$) k remains constant, but its value depends on the concentration of suspended materials, decreasing with increasing concentration. In an unsteady shear flow of clear water over a hydraulically smooth bed (Ref 5) and a rough bed (Ref 6) it was shown that the velocity profiles are logarithmic with k=0.4. The applicability of the logarithmic profile expressed by Eq (1) in the boundary layer region of the present tidal flow with suspension will be examined.

It was mentioned previously that the mean velocity profiles were measured within 1.40m from the bed, starting at z=0.125m. Total water depths 2m $< D < 5$m for two flood flows and 4m $< D < 8$m for two ebb flows. This implies that the measured height was well within the logarithmic region by assuming that there is an analogy between the estuarine flow and steady boundary layer shear flow.

The measured velocities, obtained from the 5 Braystoke current meters were plotted against their height on a semi-log paper, and the results are shown in Figs 4 to 7, indicating that the velocity profiles are logarithmic with various slopes within 1.40m height. As may be seen the logarithmic layer exceeds the 0.25D limit mentioned previously for a steady boundary layer shear flow of clear water. Moreover, Hamilton et al (Ref 13) have shown that the log-profile agrees reasonably well with the measured profile practically throughout the water depth D over 85% of the tidal cycle. Hence Eq (1) was fitted to the measured profiles by a least squares regression within 95% confidence limits (Refs 8 and 14). By choosing a zero-plane (Ref 15) for each profile to obtain the best fit with the correlation $R^2 \approx 0.996$, it was possible to calculate the friction velocity $U_*$ by assuming that the Karman constant k=0.4. The results of these evaluations are shown in Figs 8 -10, together with variations of the mean velocity U at z = 1.40m with the water depth D and the salinity S during the measuring periods. In Figs 8-10 are also shown values of the Reynolds stress $(\overline{uw})^{\frac{1}{2}}$ obtained from the EMC heads at z=0.35m, 0.95m and 1.40m. Figs 8 and 9 show that the values of $U_*$ agree reasonably well with those of $\overline{(uw)}^{\frac{1}{2}}$ at z=0.35m in the peak regions of the two ebb flows; the Reynolds shear stress remains generally higher than the $U_*$ in the accelerating and decelerating phases. Hence it can be concluded that the height z=0.35m in the peak region of the two ebb flows was within the constant shear-layer, within which the Karman constant k=0.4 was not affected by suspension. Moreover, the flow in this region can be considered as quasi-steady flow, with $U_*$ and $z_o$ as scale quantities to specify the near-bed flow in the peak region. The results shown in Figs 8 and 10 indicate that $U_* \leqslant \overline{(uw)}^{\frac{1}{2}}$ in the accelerating and decelerating phases of the two ebb flows. This implies that the flow unsteadiness affects the accelerating and decelerating phases of the ebb flow by assuming that the effect of suspension on the Karman constant is negligably small, as was the case in the peak region. A similar conclusion can be drawn from the results of a simulated two-dimensional tidal flow of clear water investigated by Anwar et al (Ref 5). Due to lack of measurements in the large part of the flood tide shown in Fig 10, it is difficult to examine the effect of the unsteady flow on the relationship between $U_*$ and $\overline{(uw)}^{\frac{1}{2}}$. It, however, appears that the trend between $U_*$ and $\overline{(uw)}^{\frac{1}{2}}$ is very similar to that obtained for the ebb flow. Figs 8 to 10 further show that the Reynolds stress decreases with increasing z, and the $\overline{(uw)}^{\frac{1}{2}}$ values are almost the same at z=0.95m and 140m.

From the results shown in Figs 8 and 9 it is difficult to concede that the constant shear layer in the peak region did extend much beyond $z \approx 0.35$m, although the thickness of the log-layer was in the order of 1.40m. Hence, it is reasonable to assume that the log-profile can hold to a larger depth, possibly to a good approximation throughout the water depth, as was the case of the experimental results obtained by Hamilton el al as discussed previously (Ref 13). The values of the bed roughness height $z_o$ are also shown in Fig 8 to 10 which indicate that the bed roughness is time dependent, This, in turn, can be attributed to the suspension of solids, which varied with time (to be shown later), and also changes in the ripple dimensions. From the results shown in Figs 8 to 10 it can be deduced that the drag coefficient $C_D$ = $(U_*/U_{z=1.40})^2$ is also time- dependent; a similar result was obtained elsewhere (Ref 6).

Figs 8 and 9, and, to a certain extent, Fig 10 indicate that the maximum of the Reynolds shear stress, and the friction velocity $U_*$ lag the peak velocity $U_{z=1.40}$, with the conclusion that the values of these parameters, being time-dependent, are not the same in the accelerating and decelerating phases of the tidal current, hence the hystersis effect which will be discussed later.

## 4.2 Turbulence Intensities

The rms horizontal velocity $(\overline{u^2})^{\frac{1}{2}}$ and that of the vertical velocity $(\overline{w^2})^{\frac{1}{2}}$ were evaluated from the measured data; their turbulence intensities, using $(\overline{uw})^{\frac{1}{2}}$ at z=0.35m as a scale quantity, are displayed in Figs 11 to 12 for two spring ebb tides and in Figs 13 for a spring flood tide. Figs 11 to 13 show that turbulence intensities in both directions, being large at z=0.35m, decrease with increasing z as is to be expected. There is no obvious reason for the substantially low horizontal turbulence intensity at z=0.35m of the 7 June ebb tide (see Fig 11). The horizontal turbulence intensities, embracing as they do a wide range of eddy sizes, are lower in the accelerating phases than those when the currents were decelerating in the ebb tides shown in Figs 11 and 12, implying that the development of eddies was completed when the flow passed the peak region. Comparable information cannot be obtained from the results of the flood tide shown in Fig 13, due to lack of measured data when the flow was decelerating. It is interesting to note that the vertical turbulence intensities, containing mainly the contribution of large eddies (Ref 9), remain almost unchanged in the accelerating and decelerating phases (see Figs 11 and 12). These figures further show that the differences between the turbulence intensities in the vertical direction at z=0.95m and z=1.40m are very small, this is not the case for the horizontal turbulence intensity, implying that the contribution of small eddies decreased with increasing z.

## 5 SUSPENSION DISTRIBUTION

### 5.1 Sand grains $d_{50} < 40\mu$

From the measured instantaneous solids concentration $C_i$, using infra-red suspended solids heads, the mean concentration $\overline{C}$ and its rms value were evaluated. It was found that $\overline{C} \approx 0.03 kg\ m^{-3}$ at z=0.125m and 0.35m with the rms values in the order of $0.001 kg\ m^{-3}$ remained the same throughout the tidal period. Similar values were obtained from some measurements made near the free surface. It can therefore be concluded that sand grains of about 40 µm remained in suspension throughout the water depth most of the time.

### 5.2 Sand grains $40\ \mu m < d_{50} < 250\ \mu m$

From the three pump sample nozzles the mean concentration C of suspended solids for grain sizes ranging between 40 µm and 250 µm was determined at z=0.125m and 0.95m. Fig 14 shows a typical cumulative size distribution. The measured mean concentration C for two spring ebb tides, and two flood tides are shown in Figs 15 to 18, in which are also given the variation of the mean velocity U at the relevant height z. Figs 15 to 18 generally disclose that the concentration C increased with increasing mean velocity U, reaching a maximum later than that of U, it then decreased as the velocity decreased. Similar patterns can be obtained for the mean sediment concentration C and its flux, UC, in the mean flow direction, and also for the turbulent kinetic energy $\overline{q^2} = (\overline{u^2} + \overline{w^2})$ which are shown in Figs 15, 16 and 18. It is noted that due to the uncertainity of the measured data at z=0.125m, as mentioned previously, the $\overline{q^2}$-values at z=0.35m are given in Figs 15, 16 and 18 by assuming that the turbulent kinetic energy at these two heights in the constant shear stress layer are very close. In other words, Figs 15, 16 and 18 disclose that the C, UC and $\overline{q^2}$ values are out of phase with the mean velocity U, resulting in the hysteresis effect which can be seen in Figs 19 for an ebb tide. As may be seen, flow parameters given in Figs 19 are higher in the decelerating flow than those when the flow is accelerating. The high $\overline{q^2}$ value during the decelerating phase is due to the large value of $(\overline{u^2})$ (see Figs 11 to 13), causing a large movement of the bed materials, which, in turn, will be picked up from the bed by $(\overline{w^2})$, which remained almost unchanged in the accelerating and decelerating phases of the current. The Reynolds shear stress, the friction velocity U* (see Figs 8 to 10), and the flow parameters shown in Figs 15, 17 and 18 are time dependent, hence dimensional arguments cannot be used for the estuarine flow as discussed previously. On the other hand, it is possible to use the one-equation turbulent model (see Appendix A), if a clear relationship can be established between the turbulent kinetic energy $\overline{q^2}$ and $\overline{uw}$. The values of $\overline{q^2}$ are plotted against $\overline{uw}$ in Fig 20 (a, b, c) during the accelerating and decelerating phases of two ebb tides and a flood tide at z=0.35m. The results given in Fig 20 do not show a hysteresis effect. Solid lines drawn by inspection in Fig 20 (excluding the last result in Fig 20c) reveal a linear relationship between $\overline{q^2}$ and $\overline{uw}$ of the following form:

$$a = -\frac{\overline{uw}}{\overline{q^2}} \qquad (2)$$

where $a \approx 0.25$ for the results given in Fig 20 (b and c) increases to $a \approx 0.45$ for the 7June ebb tide. In a two-dimensional boundary layer shear flow of hamogeneous fluid $a \approx 0.15$ (Ref 7) increasing to $a \approx 0.17$ for a two-dimensional heat transfer flow (Ref 17). The high a-value of the present data is to be expected, because the rms value of the lateral velocity component was not included in $\overline{q^2}$. The results shown in Fig 20 and Eq 2 indicate that the one-equation turbulent model can be used for estuarine flow to calculate the mean velocity components and the Reynolds shear stress (see Appendix A).

# 6 CONCLUSION

Field measurements were conducted in the estuary of the River Taw during the spring ebb and flood tides with the following results:

1 Mean velocity profiles were logarithmic within the measuring depth of 1.40m from the bed.

2 Friction velocity, with the Karman constant of 0.4, agreed well with the near-bed Reynolds shear stress in the peak region, but otherwise the Reynolds shear stress was higher than the friction

velocity in the accelerating and decelerating phases.

3 The Reynolds shear stress, being large near the bed, decreased with increasing distance from the bed. The values of the Reynolds shear stresses were practically the same at elevations 0.95m and 1.40m.

4 In the decelerating phase the horizontal turbulence intensities were higher than those in the accelerating phases. The turbulence intensities in the vertical direction remained the same in the accelerating and decelerating flows.

5 The turbulence intensities in the vertical and horizontal directions, being large near the bed, decreased as the distance from the bed increased.

6 Sand grains of about 40 μm remained in suspension throughout the depth during the measuring tidal cycles.

7 The concentration of sand grains with $d_{50}$ varying between 40 μm and 250 μm, was out of phase with the mean velocity variation. It increased and then decreased with the increase and decrease of the mean velocity, producing a hysteresis. Similar hysteresis patterns were obtained for the horizontal sediment flux and the turbulent kinetic energy.

8 Variation of the turbulent kinetic energy was in phase with the increase and decrease of the Reynolds shear stress without a hysteresis effect.

## 7 APPENDIX A

The turbulent energy closure numerical simulation is based on the turbulent energy equation, which can be written in the following form for a two-dimensional unsteady flow:

$$\tfrac{1}{2}\rho\frac{\partial\overline{q^2}}{\partial t} + \rho\left(U\frac{\partial}{\partial x}+W\frac{\partial}{\partial z}\right)\overline{q^2} - \tau\frac{\partial U}{\partial z}+\frac{\partial}{\partial z}\left(\overline{pw}+\tfrac{1}{2}\rho\,\overline{q^2 w}\right) + \rho\varepsilon = 0 \quad (1A)$$

advection production diffusion dissipation

in which it is assumed that the Reynolds number is sufficiently high to neglect the viscous term. Eq (1A) indicates the rate of turbulent kinetic energy along a streamline. The experimental results of the present study revealed that the ratio $\frac{\tau}{\rho\overline{q^2}} = a$ remains constant for a given flow, hence Eq (1A) can be written as:

$$\frac{\partial}{\partial t}\left(\frac{\tau}{2\rho a}\right) + \left(U\frac{\partial}{\partial x}+W\frac{\partial}{\partial z}\right)\left(\frac{\tau}{2\rho a}\right) - \frac{\tau}{\rho}\frac{\partial U}{\partial z} + \frac{\left(\frac{\tau}{\rho}\right)^{3/2}}{L} = 0 \quad (2A)$$

In Eq (2A) it is assumed that, to a first approximation, the diffusion term is small, and the existance of the local-equilibrium, ie the turbulent production is equal to dissipation; which leads to

$\varepsilon = \frac{\left(\frac{\tau}{\rho}\right)^{3/2}}{L}$ , where L can be approximated to the mixing length.

The boundary layer momentum equation in the horizontal direction will be:

$$\rho\frac{\partial U}{\partial t} + \rho\left(U\frac{\partial U}{\partial x} + W\frac{\partial U}{\partial z}\right) = -\frac{1}{\rho}\frac{\partial P}{\partial x} + \frac{\partial\tau}{\partial z} \quad (3A)$$

Eqs (2A) and (3A) together with the continuity equation, ie

$$\frac{\partial U}{\partial x} + \frac{\partial W}{\partial z} = 0 \tag{4A}$$

will form a set of three equations to calculate U, W and $\tau$.

It is to be noted that a transport equation similar to (1A) can be written for the suspended solids transport to calculate the flux UC in the accelerating and decelerating phases of the flow.

## 8 REFERENCES


1 Sternberg, R W, Friction factors in tidal channels with different bed roughness. Marine Geology, 6, 1968, pp 243-260.

2 Rossiter, J S, and Lennon, G W, Computation of tidal conditions in the Thames estuary by the initial value method. Proceedings of the Institute of Civil Engineers, 31, 1965, pp25-56.

3 Celik, J and Rodi, W, Mathematical modelling of suspended sediment transport in open channels. 21st Congress, International Association for Hydraulic Research, Vol 3, Melbourne, Australia, 1985, pp534-538.

4 Thorn, M F C, Deep tidal flow over a fine sand bed. 16th Congress, International Association for Hydraulic Research, A27, Sào Paulo, 1975, pp217-223.

5 Anwar, H O, and Atkins R, Turbulence measurements in simulated tidal flow. Proceedings ASCE, Hydraulics division, Vol 106, No HY8, 1980, pp1273-1289.

6 Anwar, H O, A study of the turbulence structure in a tidal flow. Coastal and Shelf Science, 13, 1981, pp373-387.

7 Bradshaw, P, Ferriss, D M and Atwell, N P, Calculation of the boundary-layer development using the turbulent energy equation. Journal of Fluid Mechanics, 28, 1967, pp593-616.

8 Gross, T F, and Norwell, A R M, Mean flow and turbulence scaling in a tidal boundary layer.

Continental Shelf Research, Vol 2, No 2/3, 1983, pp109-126.

9 Anwar, H O, and Atkins R, Turbulent structure in an open-channel flow. Proceedings of Euromech 156/Mechanics of Sediment Transport/Istanbul/12-14 July 1982, pp19-25.

10 Monin, A S, and Yaglom, A M, Statistical Fluid Mechanics: Mechanics of Turbulence, ed by J L Lumley, Vol 1, Third printing, 1977, pp412-416.

11 Elata, C and Ippen, A T, The dynamics of open-channel flow with suspension of naturally buoyant particles. MIT Hydro, Lab, Tech Report No 45, 1961.

12 Vanoni, V. A, Some effects of suspended sediment on flow characteristics, Proceedings 5th Hydraulic Conference University of Iowa, 1953, pp137-158.

13 Hamilton, D, Sommerville, J H, and Stanford, P N, Bottom currents and shelf sediments, southwest of Britian. Sedimentary Geology, 1980, 26 pp115-138.

14 Wilkinson, R H, A method of evaluating statistical errors associated with logarithmic velocity profiles, Geo-Marine Letters, vol 3, 1983, pp49-52.

15 Anwar, H O, Low Reynolds number turbulent flow in laboratory flume. Journal of Engineering Mechanics ASCE, Vol 112, No 1, 1986, pp55-69.

TABLE.

| Time (hr BST) | | 0900 | 0905 | 0910 | 0915 | 1035 | 1040 | 1045 | 1050 |
|---|---|---|---|---|---|---|---|---|---|
| $U_m$ ($ms^{-1}$) | a | 0.602 | 0.662 | 0.669 | 0.709 | 0.54 | 0.307 | 0.461 | 0.257 |
| | b | 0.635 | | 0.696 | | 0.405 | | 0.358 | |
| | c | 0.648 | | | | 0.424 | | | |
| $(\overline{u^2})^{\frac{1}{2}}$ ($ms^{-1}$) | a | 0.069 | 0.078 | 0.067 | 0.065 | 0.08 | 0.065 | 0.074 | 0.051 |
| | b | 0.076 | | 0.067 | | 0.106 | | 0.071 | |
| | c | 0.074 | | | | 0.125 | | | |
| $(\overline{w^2})^{\frac{1}{2}}$ ($ms^{-1}$) | a | 0.067 | 0.075 | 0.067 | 0.067 | 0.10 | 0.07 | 0.086 | 0.057 |
| | b | 0.077 | | 0.068 | | 0.109 | | 0.075 | |
| | c | 0.074 | | | | 0.124 | | | |
| $(\overline{uw})^{\frac{1}{2}}$ ($ms^{-1}$) | a | 0.0616 | 0.073 | 0.058 | 0.055 | 0.076 | 0.068 | 0.0775 | 0.05 |
| | b | 0.07 | | 0.059 | | 0.121 | | 0.0713 | |
| | c | 0.067 | | | | 0.132 | | | |

Table 1. Flow parameters for a = 5, b = 10 and c = 15 minute record lengths during the accelerating phase of the spring ebb tide, 7 June 1986, at z = 0.35m.

FIGURES.

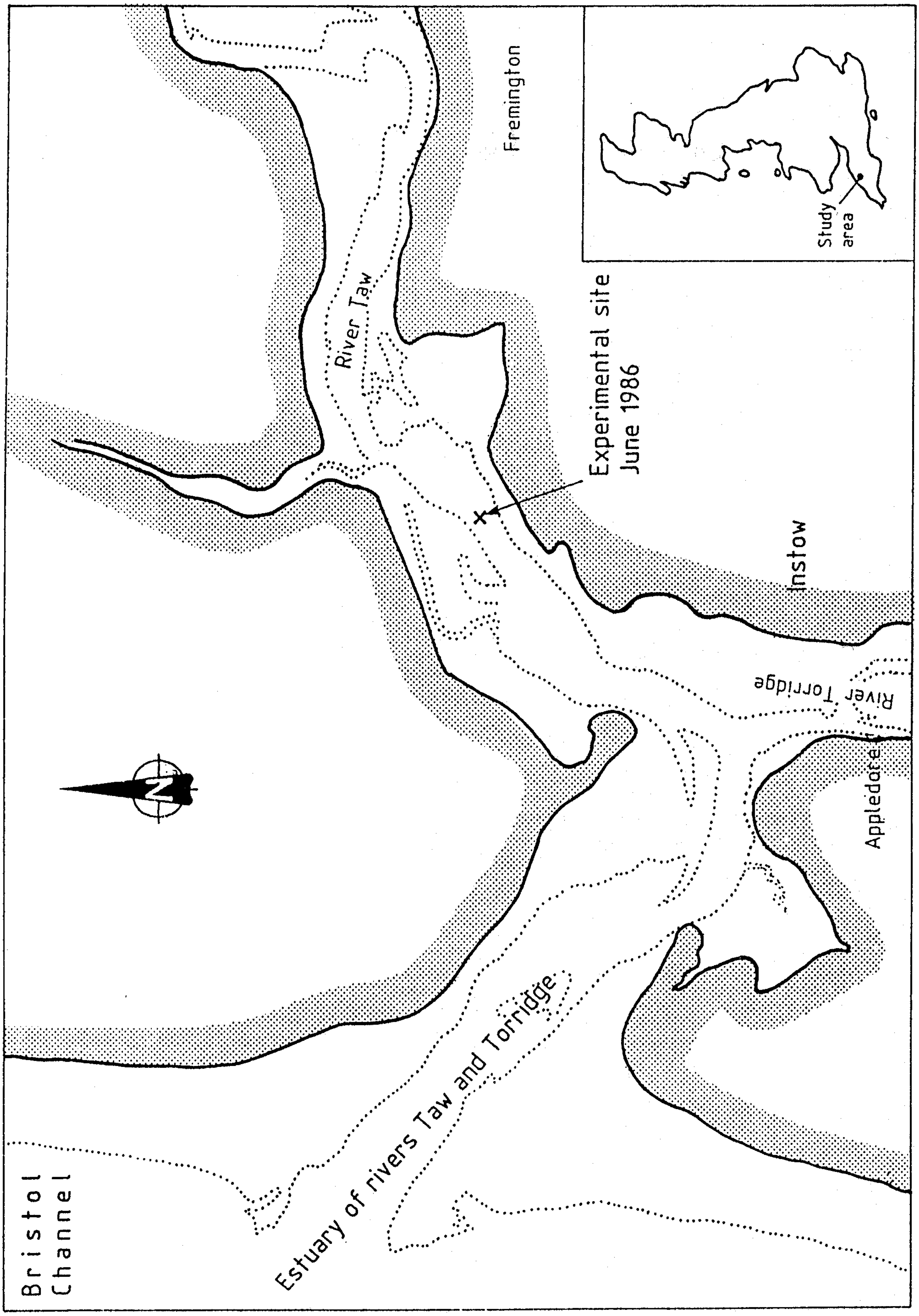


Fig 1     Location of the experimental site.

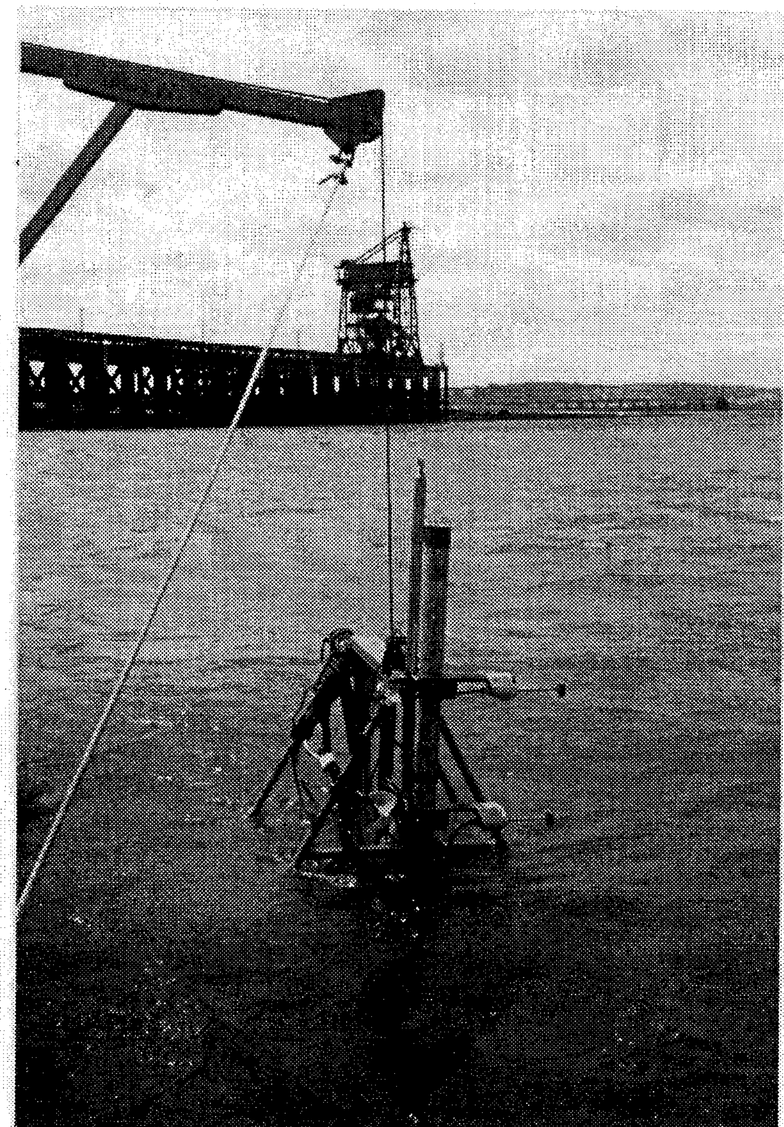

Fig 2 Experimental site and the power station jetty.

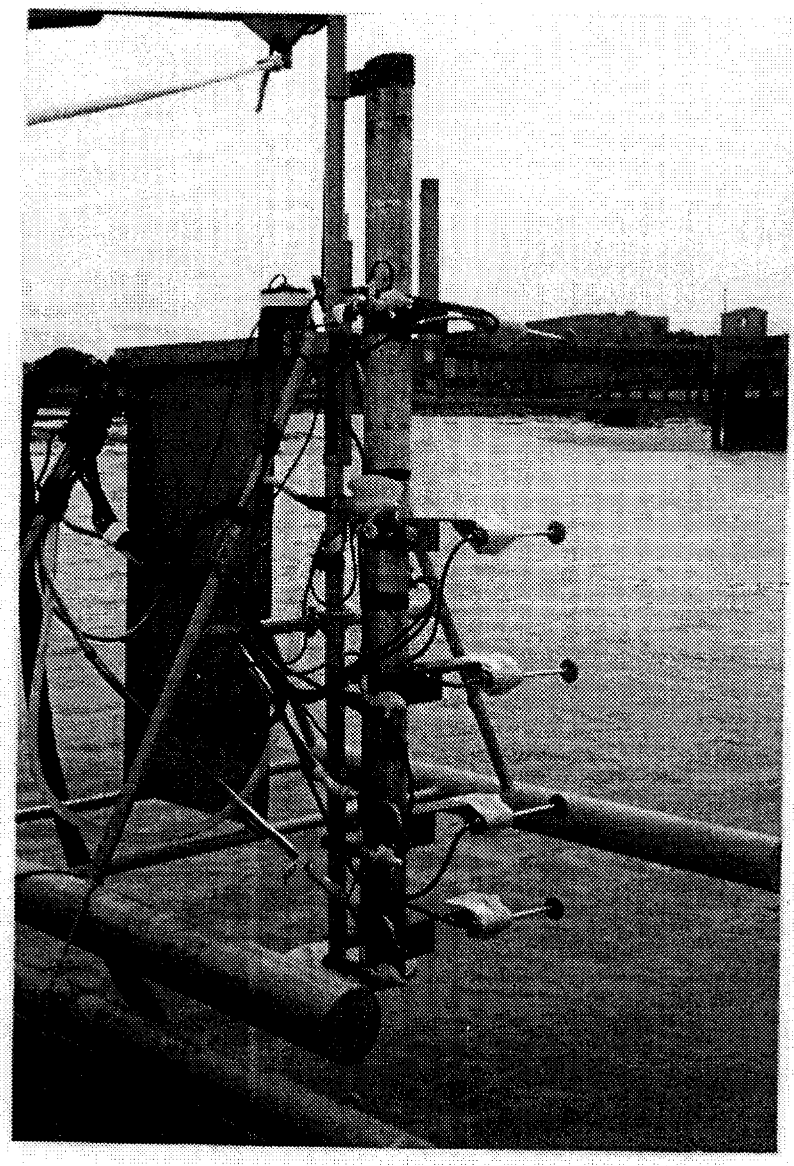

Fig 3 Bed frame with the streamlined mast supporting Electromagnetic current meters, Braystoke current meters, three infra-red suspended solids monitoring heads and three pumped sample nozzles. With vertical vane, circular base plate and a pitch and roll sensor fitted to the bed frame.

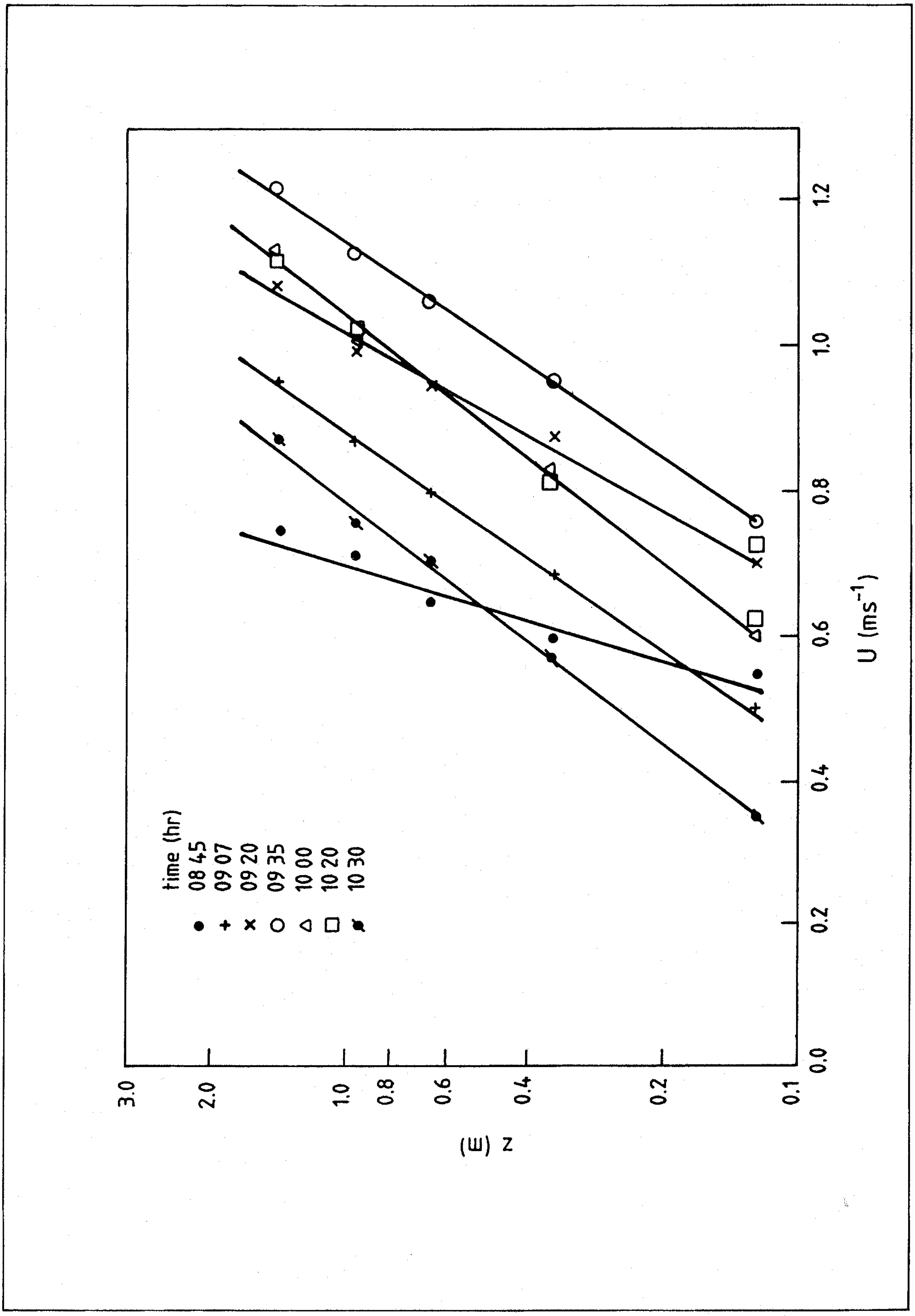


Fig 4 Mean velocity U verses height z for the ebb flow on 7 June 1986, Solid lines are logarithmic profiles.

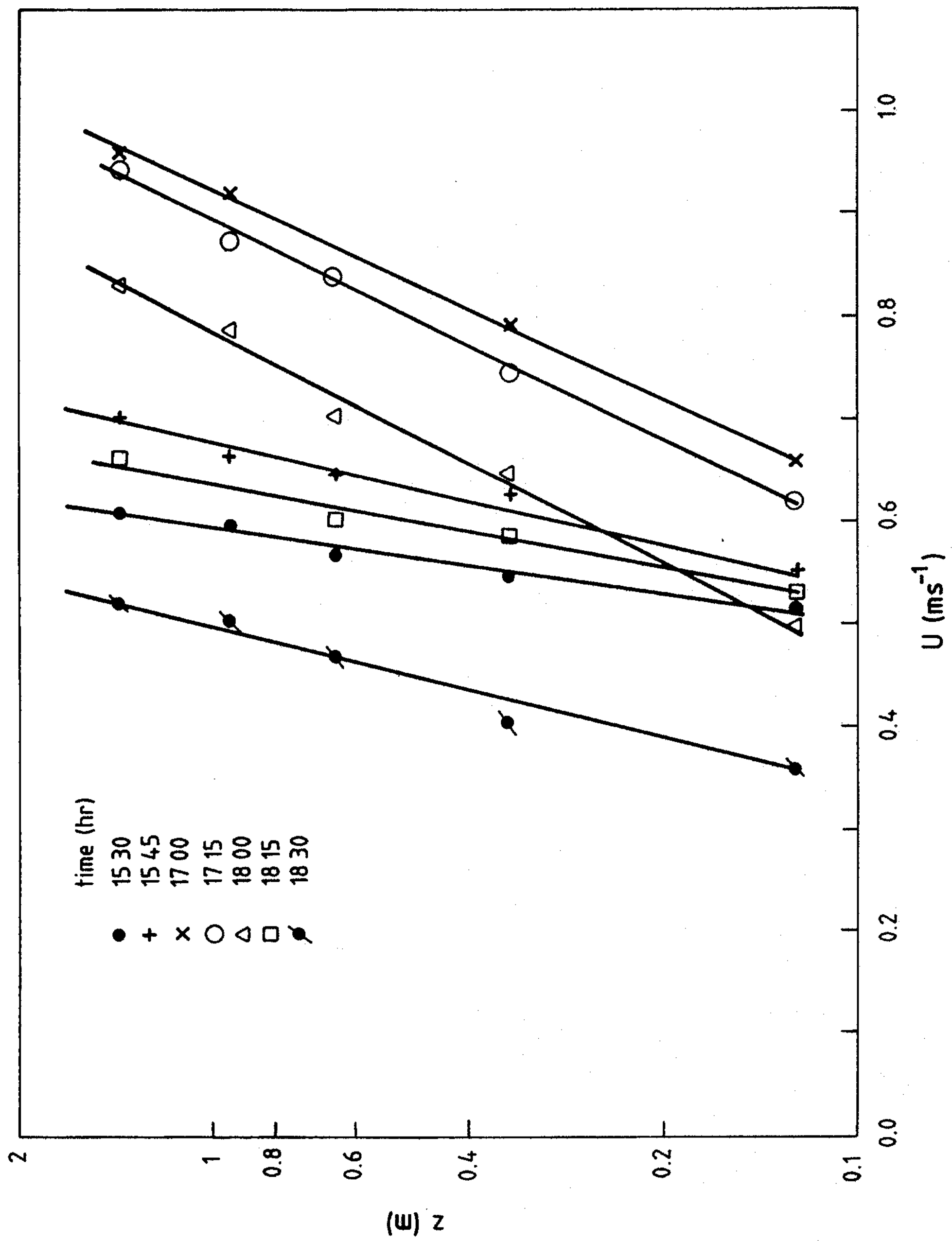


Fig 5. Mean velocity U verses height z for the flood flow, 7 June 1986, Solid lines are logarithmic profiles.

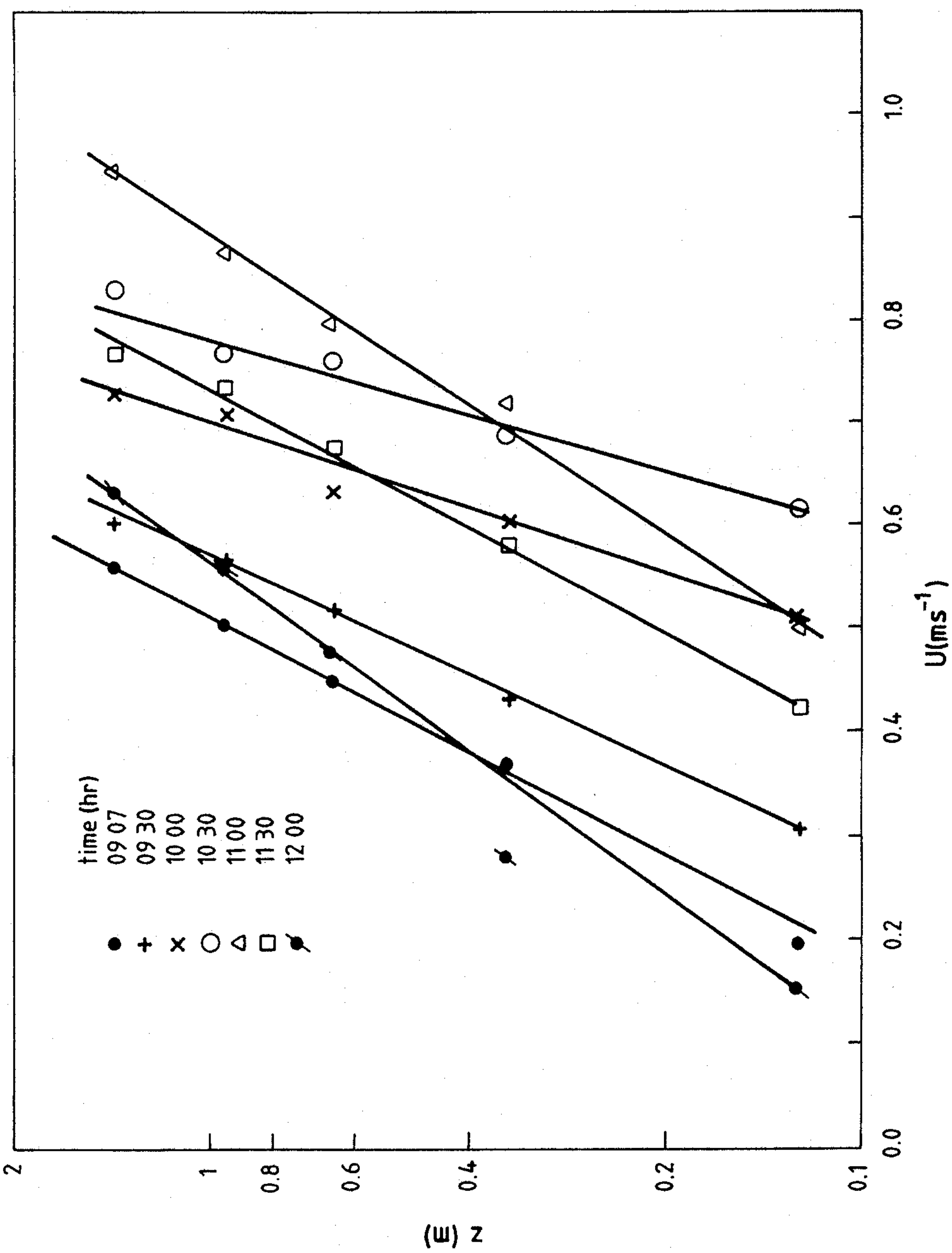


Fig 6 Mean velocity U verses height z for the ebb flow, 8 June 1986, Solid lines are logarithmic profiles.

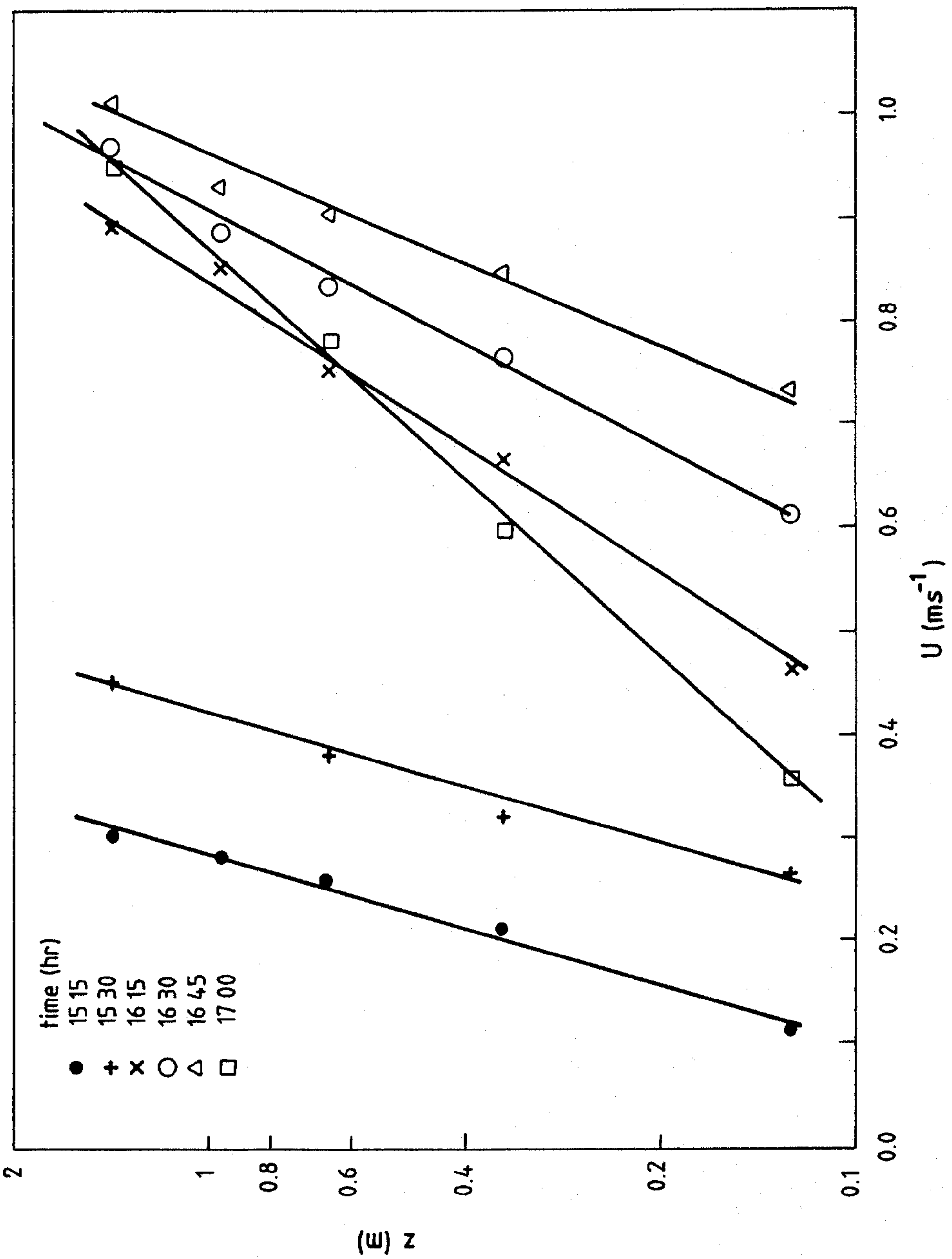


Fig 7 Mean velocity U verses height z for the flood flow, 8 June 1986, Solid lines are logarithmic profiles.

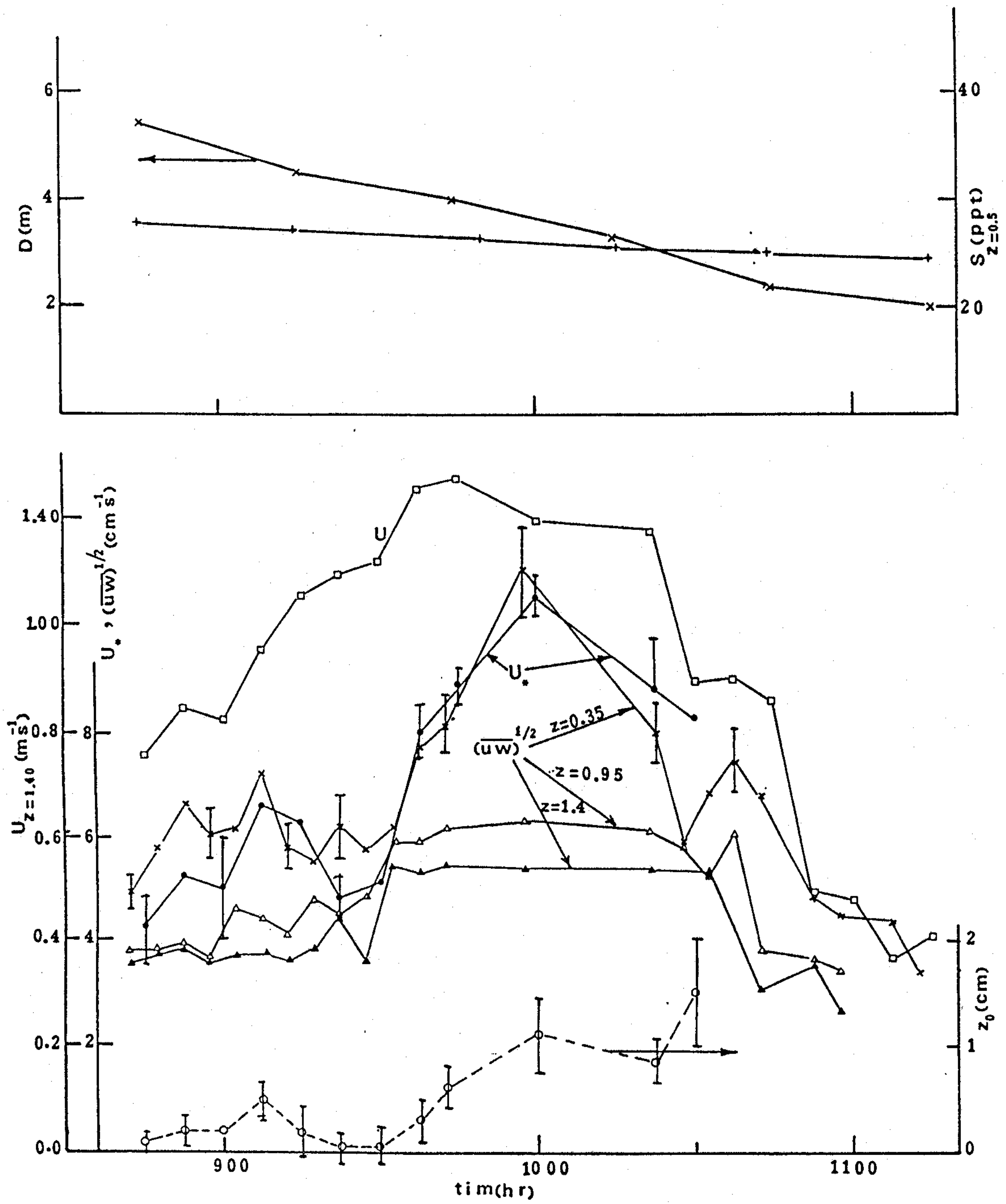


Fig 8 Variation of mean velocity U, friction velocity $U_*$, Reynolds shear stress $(uw)^{1/2}$ at three heights, roughness height $z_0$, salinity S and the water depth D during the ebb tide, 7 June 1986.

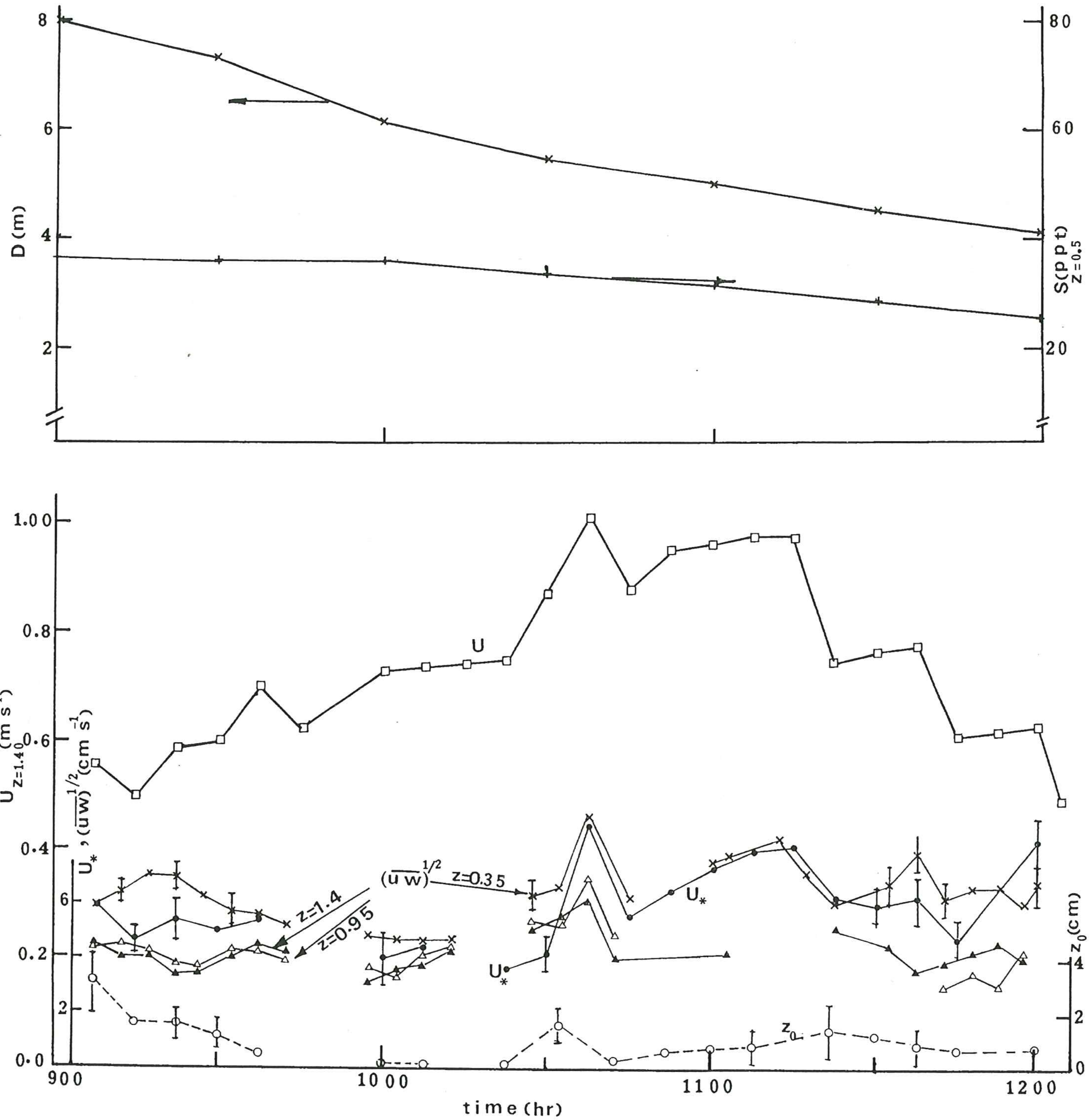


Fig 9 Variation of mean velocity U, friction velocity $U_*$, Reynolds shear stress $(uw)^{1/2}$ at three heights, roughness height $z_0$, salinity S and the water depth D during the ebb tide, 8 June 1986.

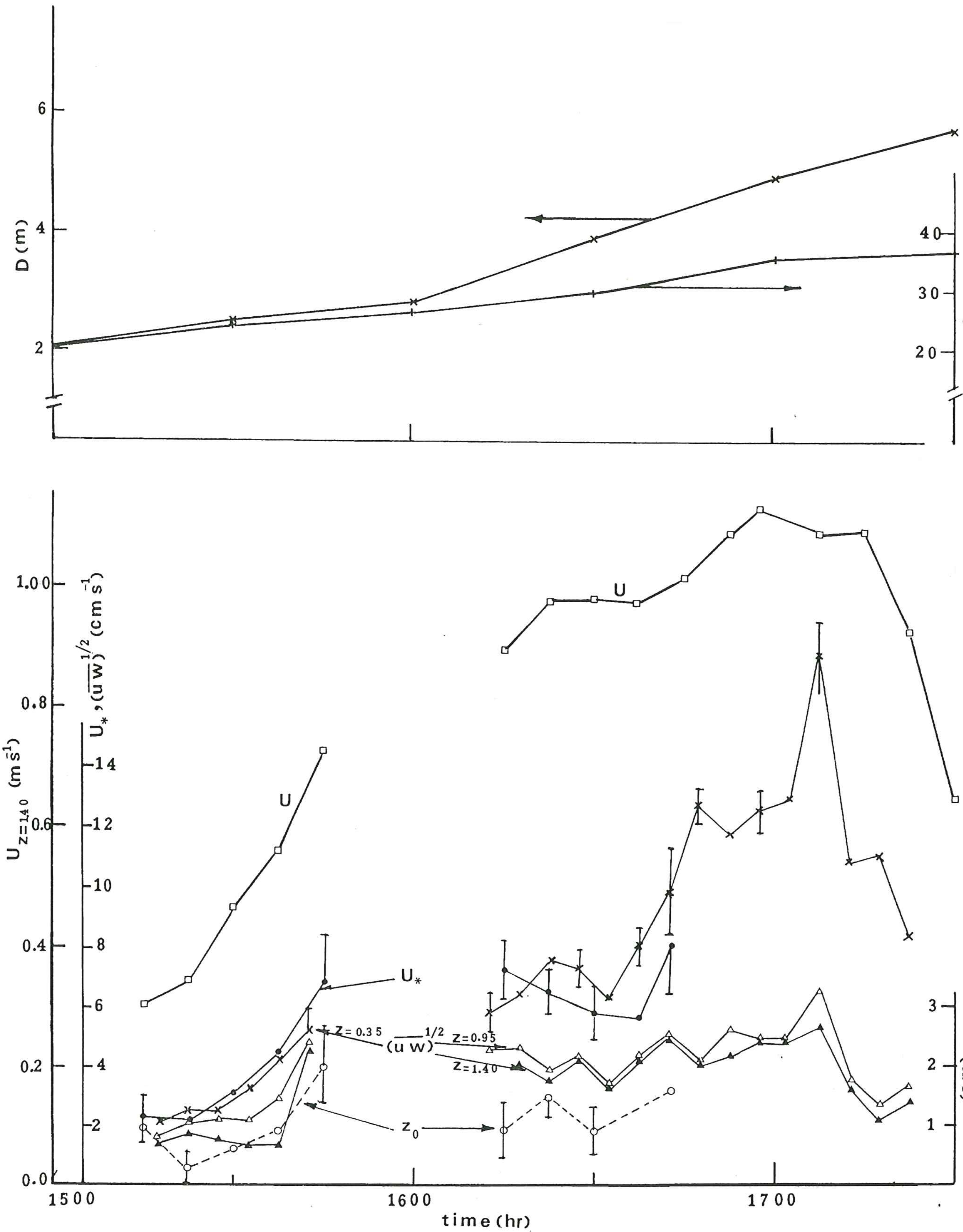


Fig 10 Variation of mean velocity U, friction velocity $U_*$, Reynolds shear stress $\overline{(uw)}^{1/2}$ at three heights, roughness height $z_0$, salinity S and the water depth D during the flood tide, 8 June 1986.

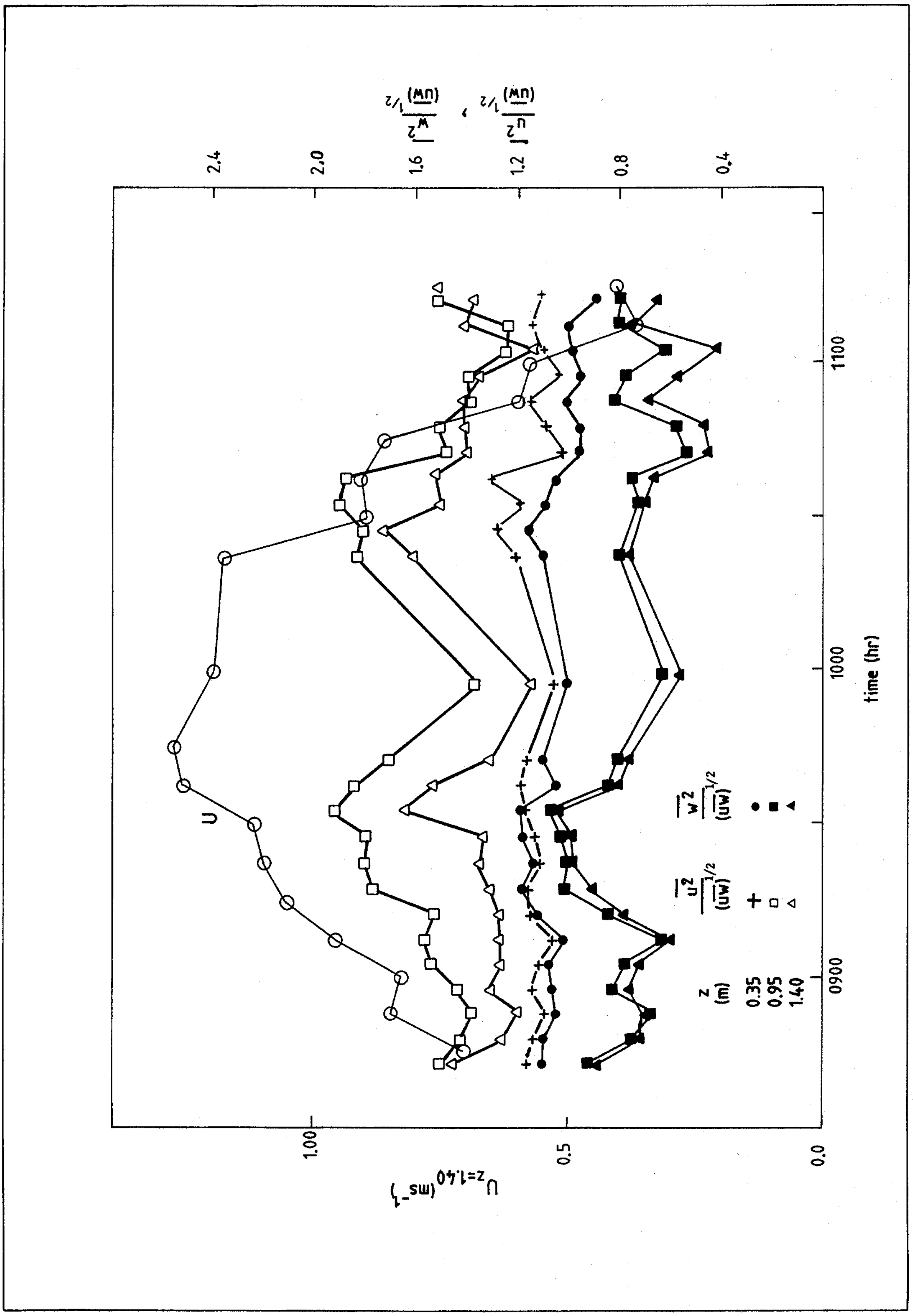


Fig 11 Variation of turbulence intensities in the horizontal and vertical directions during the ebb tides, 7 June 1986.

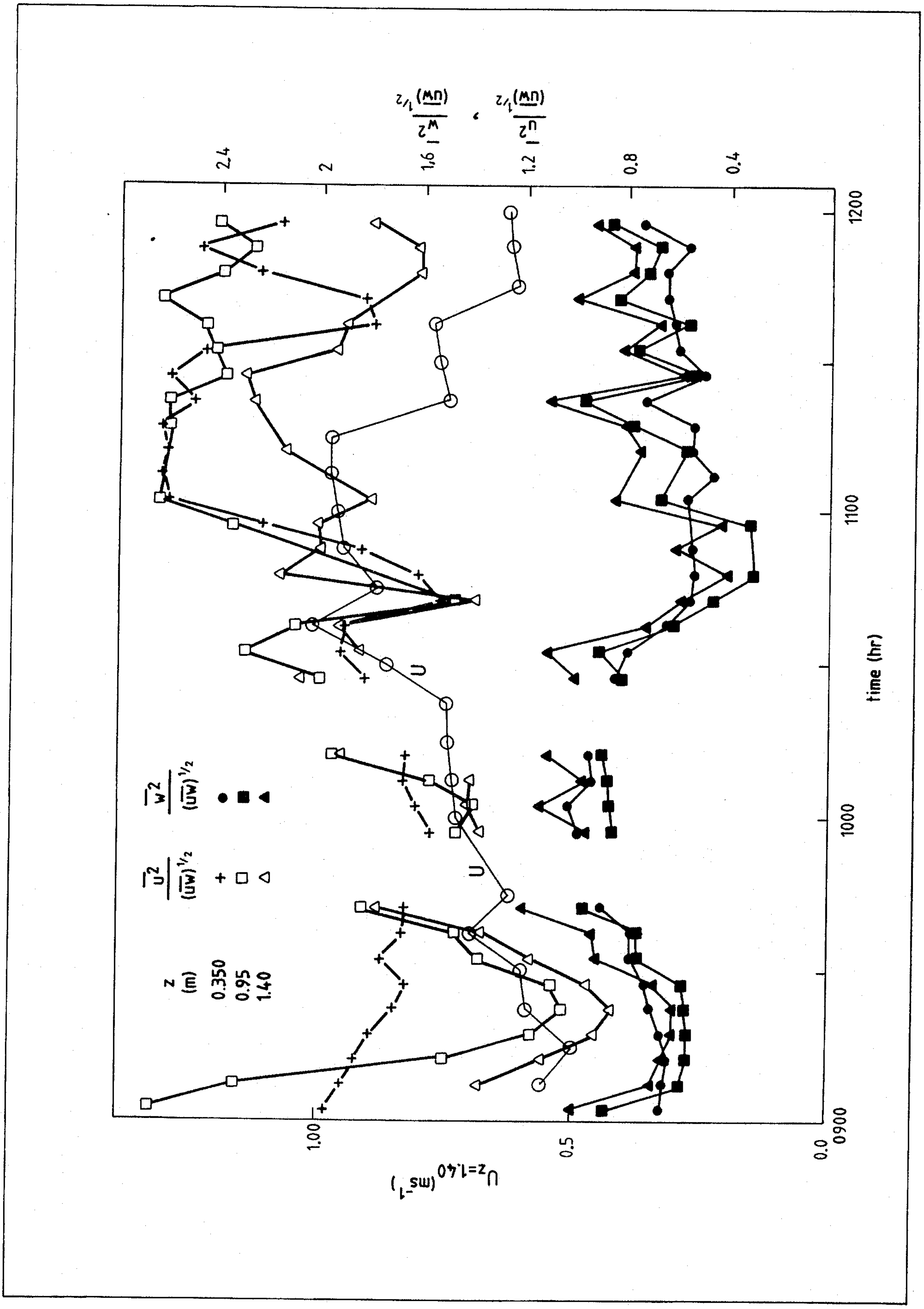


Fig 12 Variation of turbulence intensities in the horizontal and vertical directions during the ebb tide, 8 June 1986

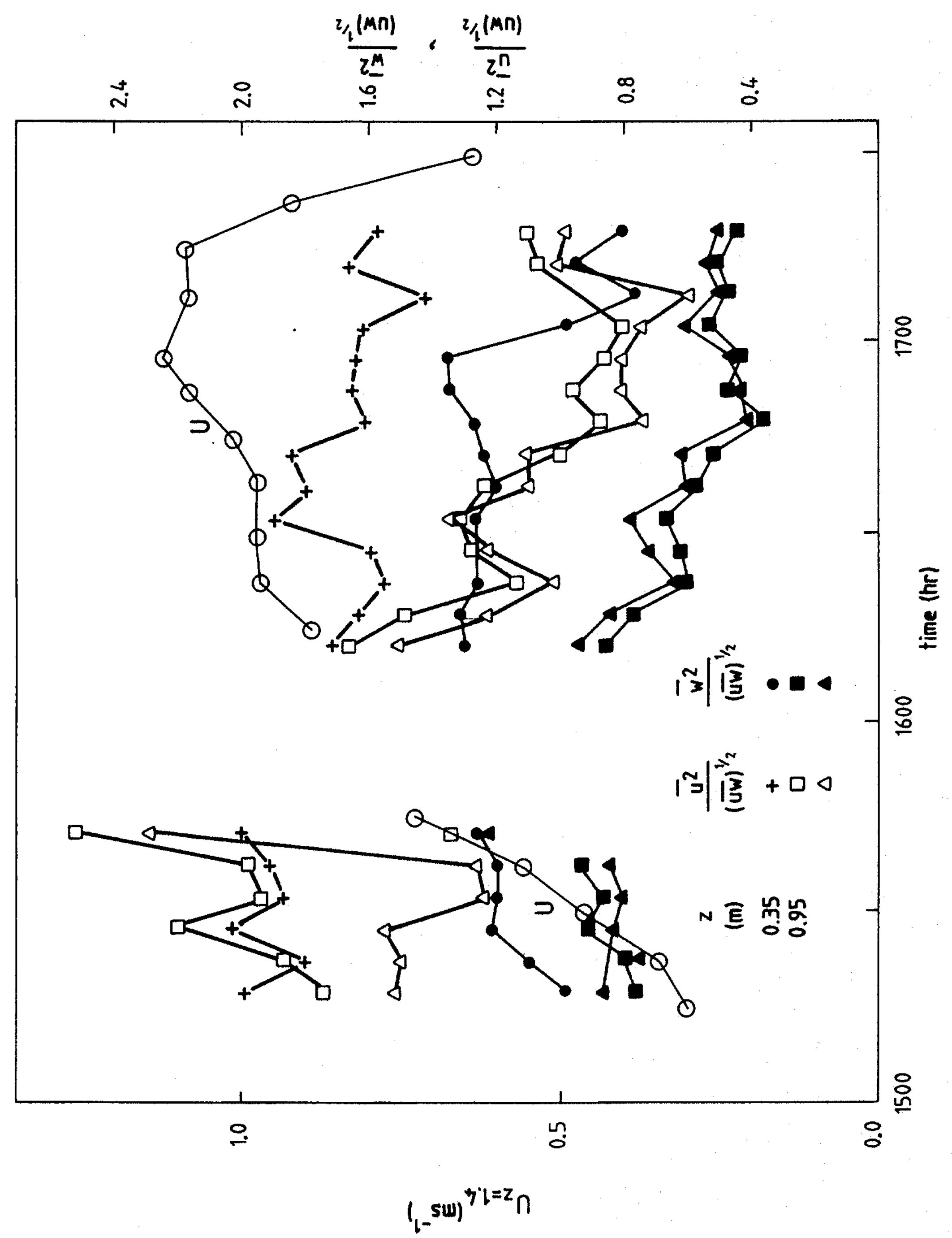


Fig 13 Variation of turbulence intensities in the horizontal and vertical directions during the flood tide, 8 June 1986.

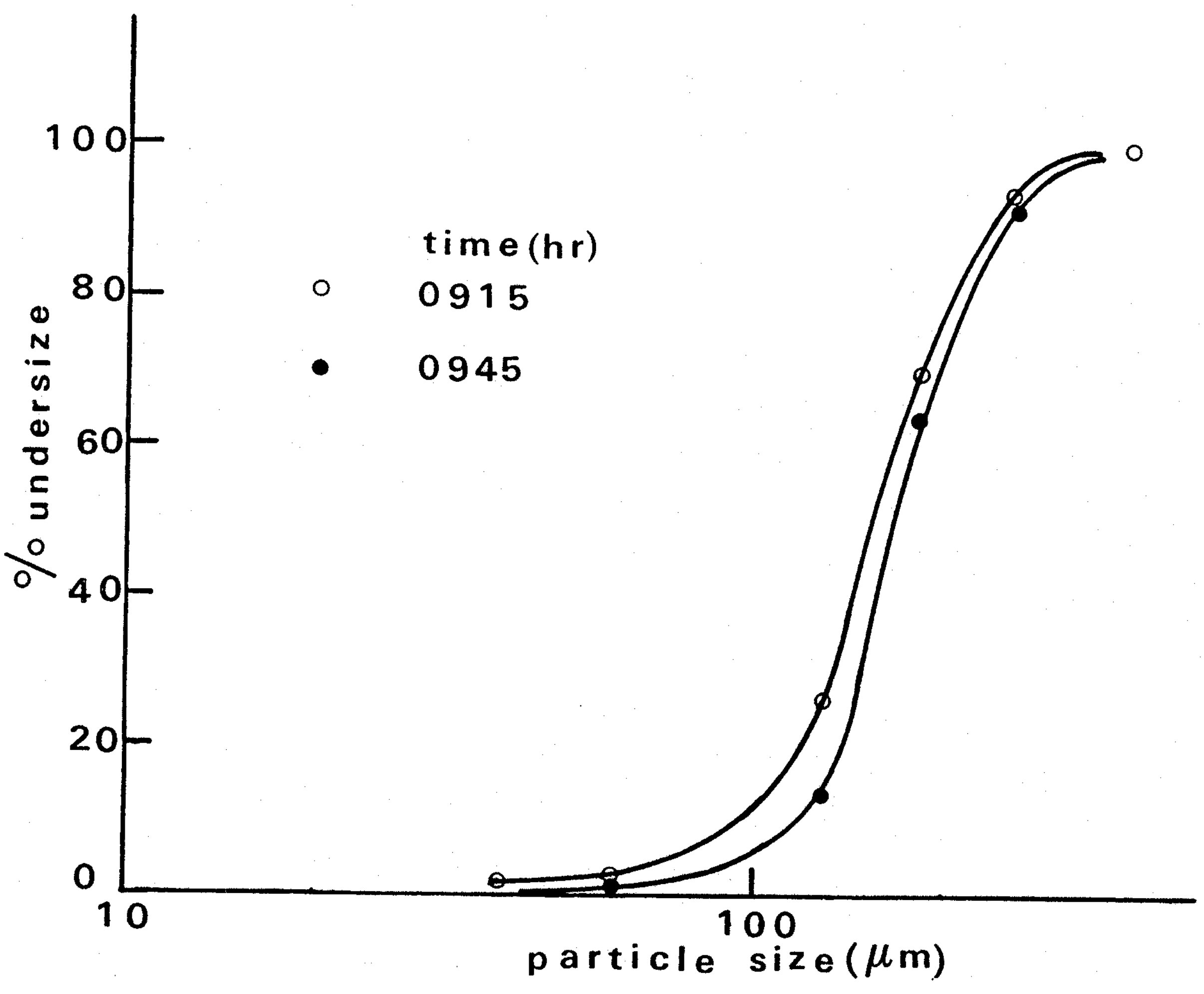


Fig 14 Cumulative grain size distributions at height z = 0.125m during the ebb tide on 7 June 1986

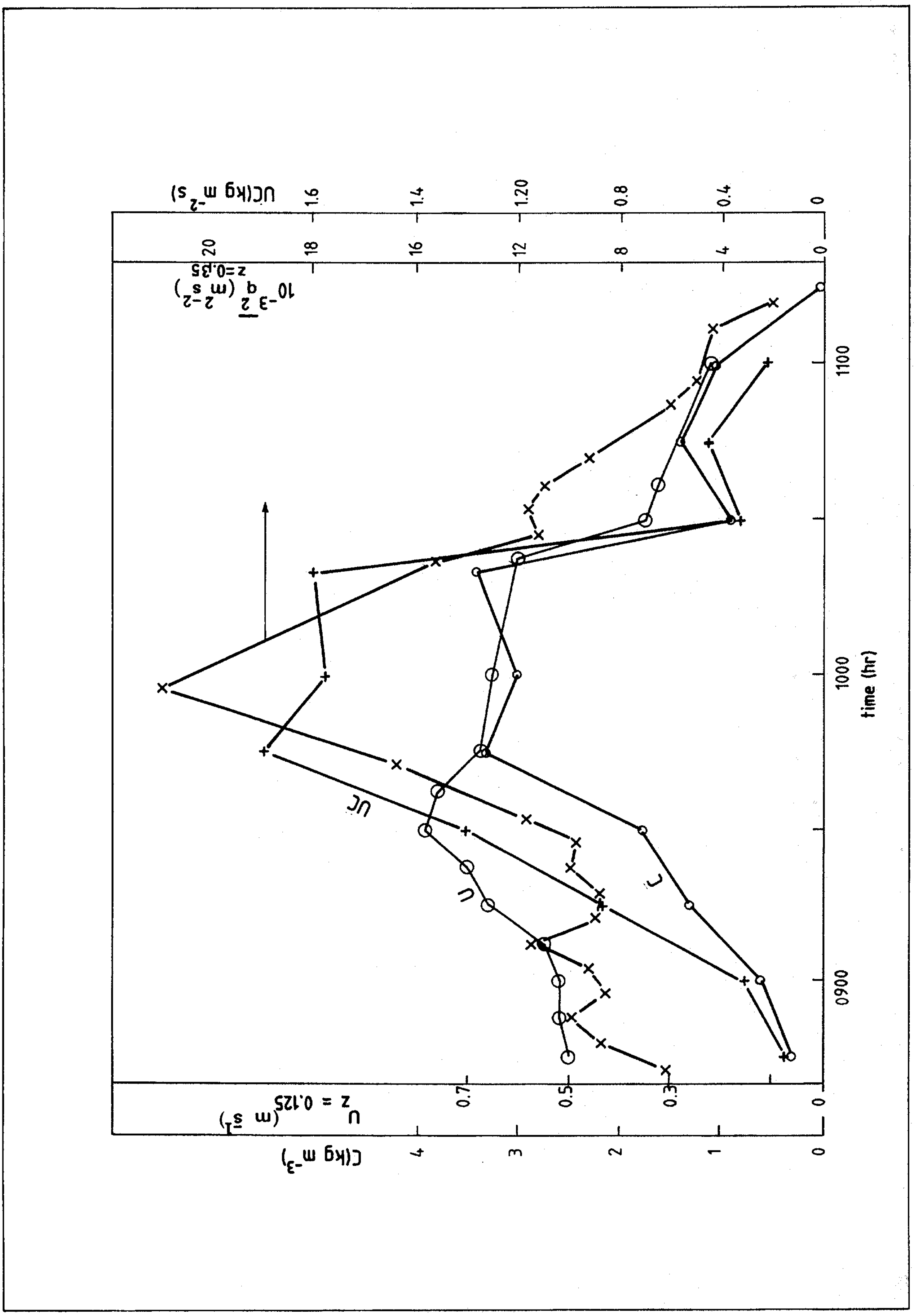


Fig 15 Variation of suspended solids mean concentration C, mean velocity $\underline{U}$, and mean flux UC at height z=0.125m, turbulent kinetic energy $\overline{q^2}$ at z=0.35 during the ebb tide, 7 June 1986.

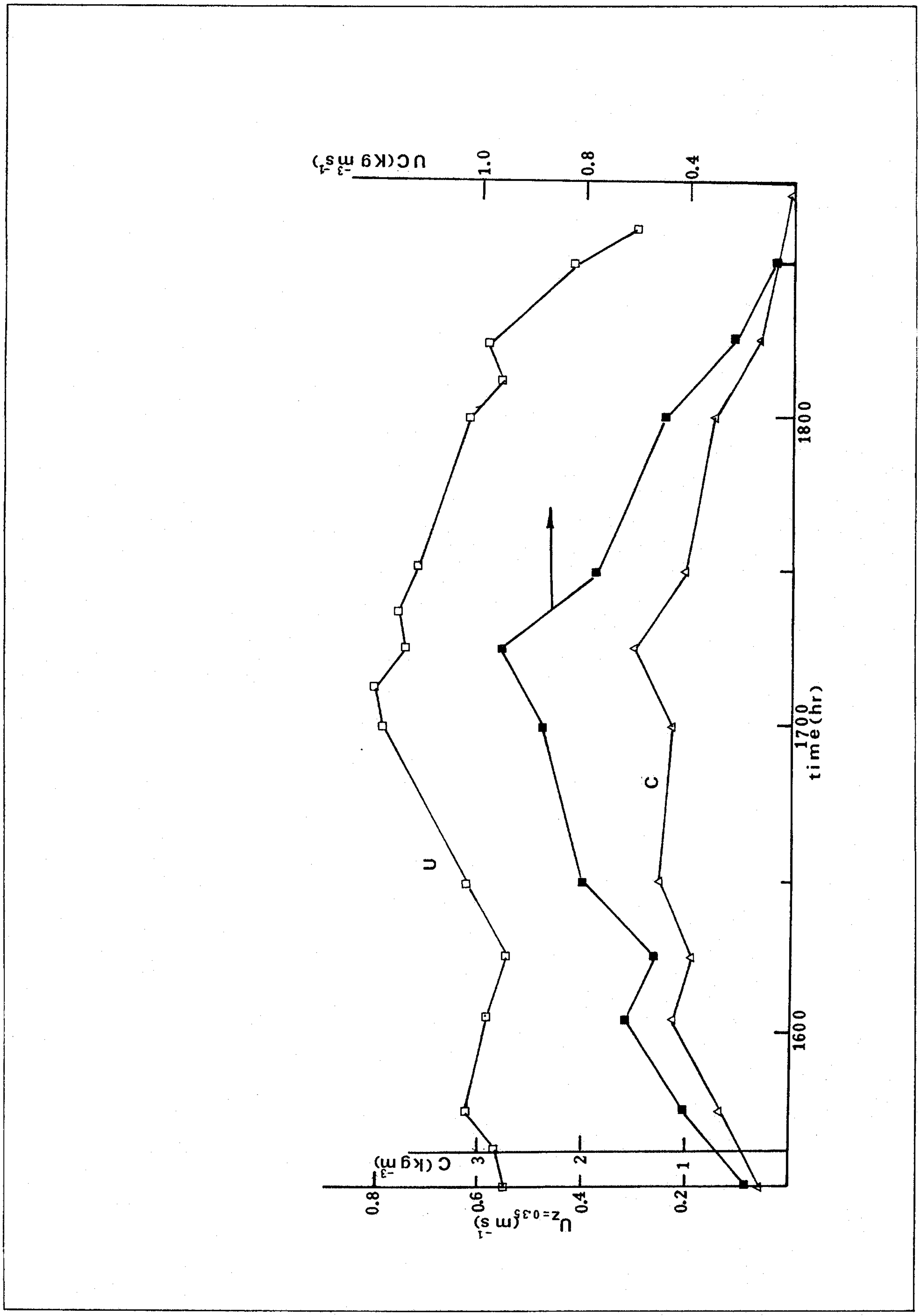


Fig 16 Variation of suspended solid mean concentration C, mean velocity U and mean flux UC at height Z = 0.35m during flood tide, 7 June 1986.

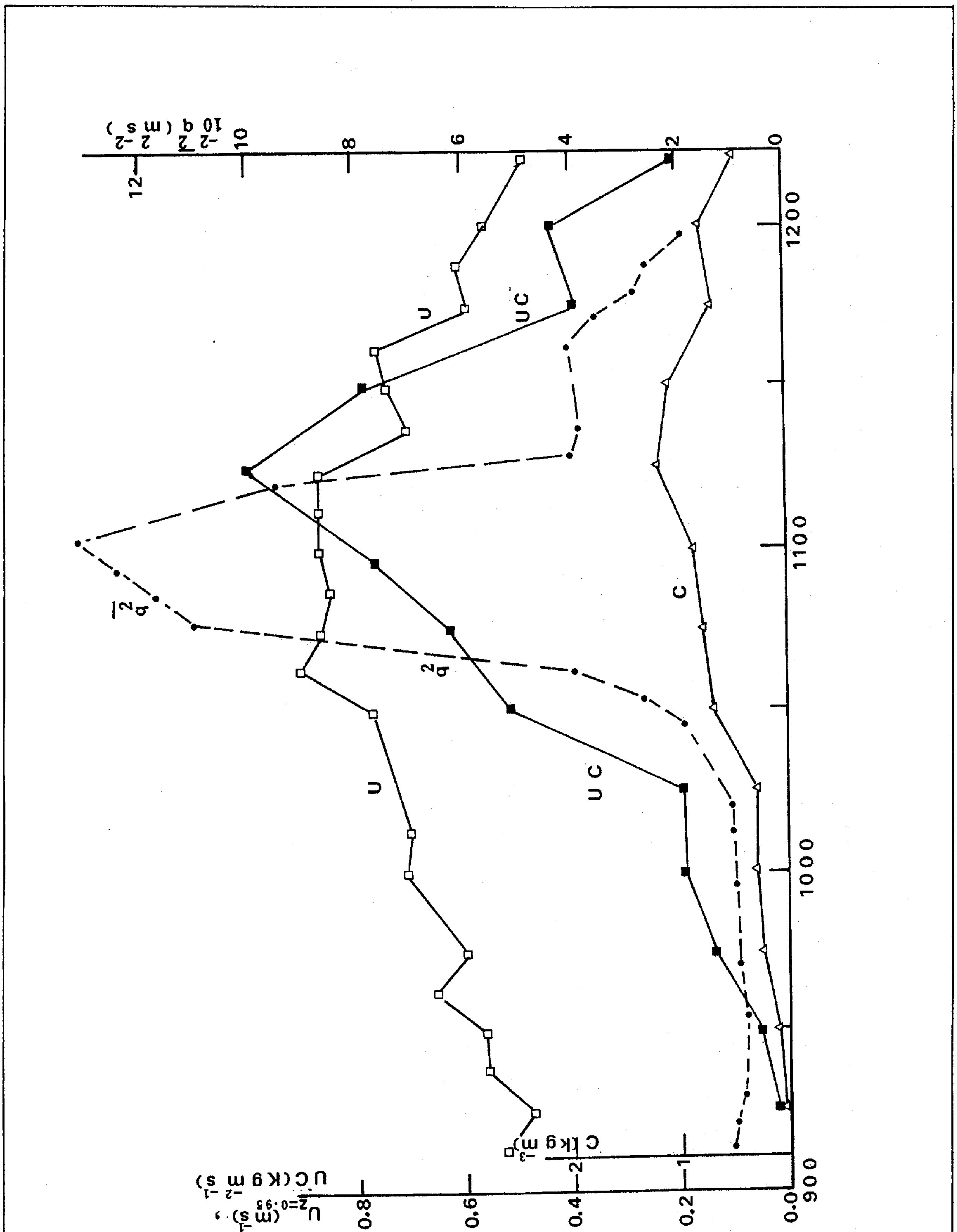


Fig 17 Variation of suspended solid mean concentration C, mean velocity U, mean flux UC and turbulent kinetic energy $\overline{q^2}$ at height z=0.95m during ebb tide, 8 June 1986.

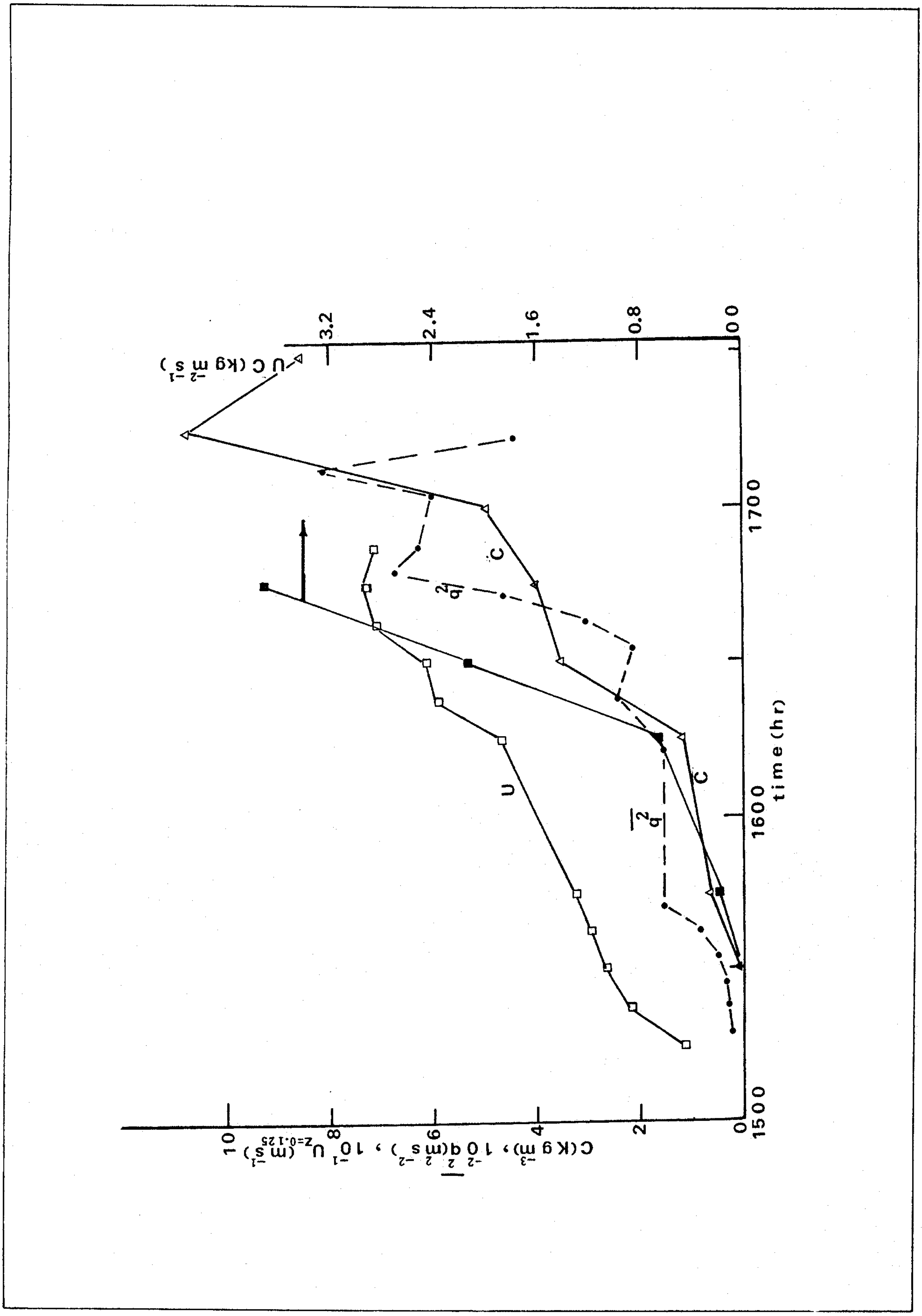


Fig 18 Variation of suspended solid mean concentration C, mean velocity U, mean flux UC at height z=0.125m, and turbulent kinetic energy $\overline{q^2}$ at z=0.35 during flood tide, 8 June 1986.

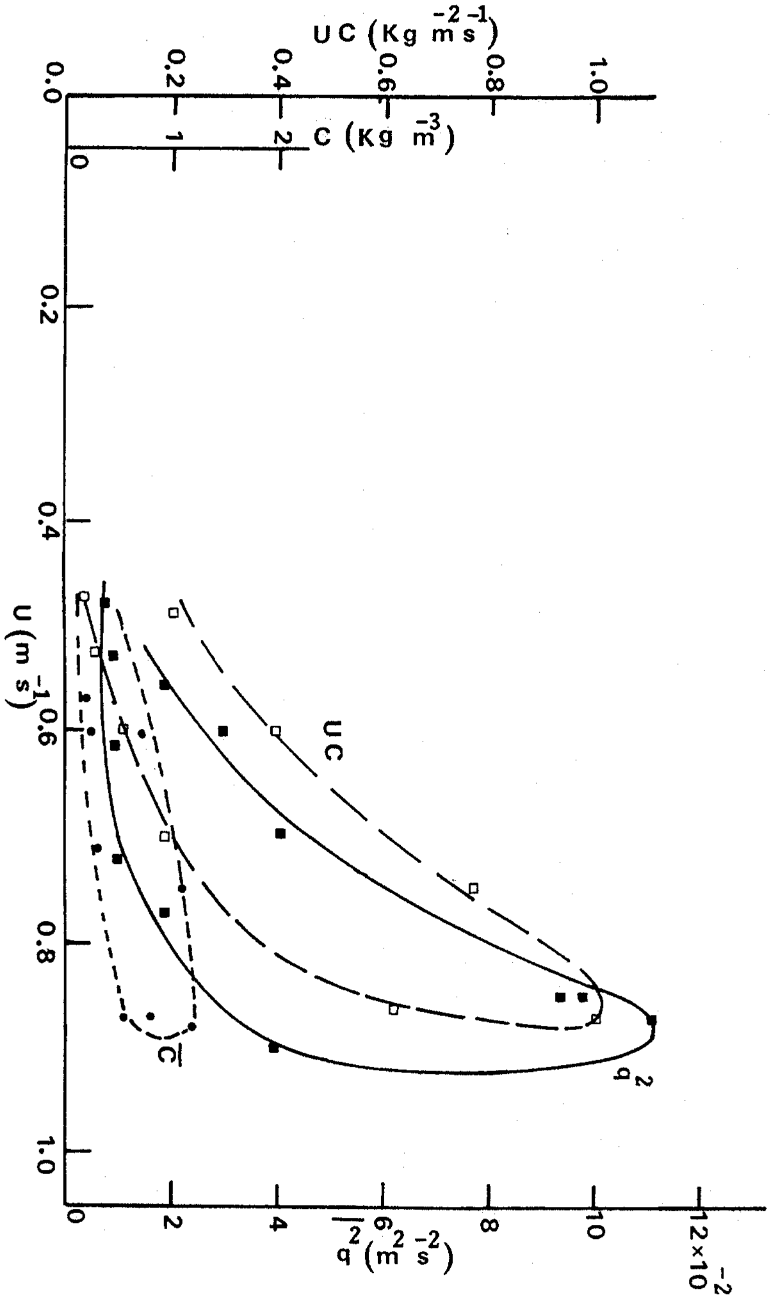


Fig 19 Hysteresis curves of suspended solids mean concentration C, mean flux UC and turbulent kinetic energy $\overline{q^2}$ at height z=0.95m for ebb flow, 8 June 1986.

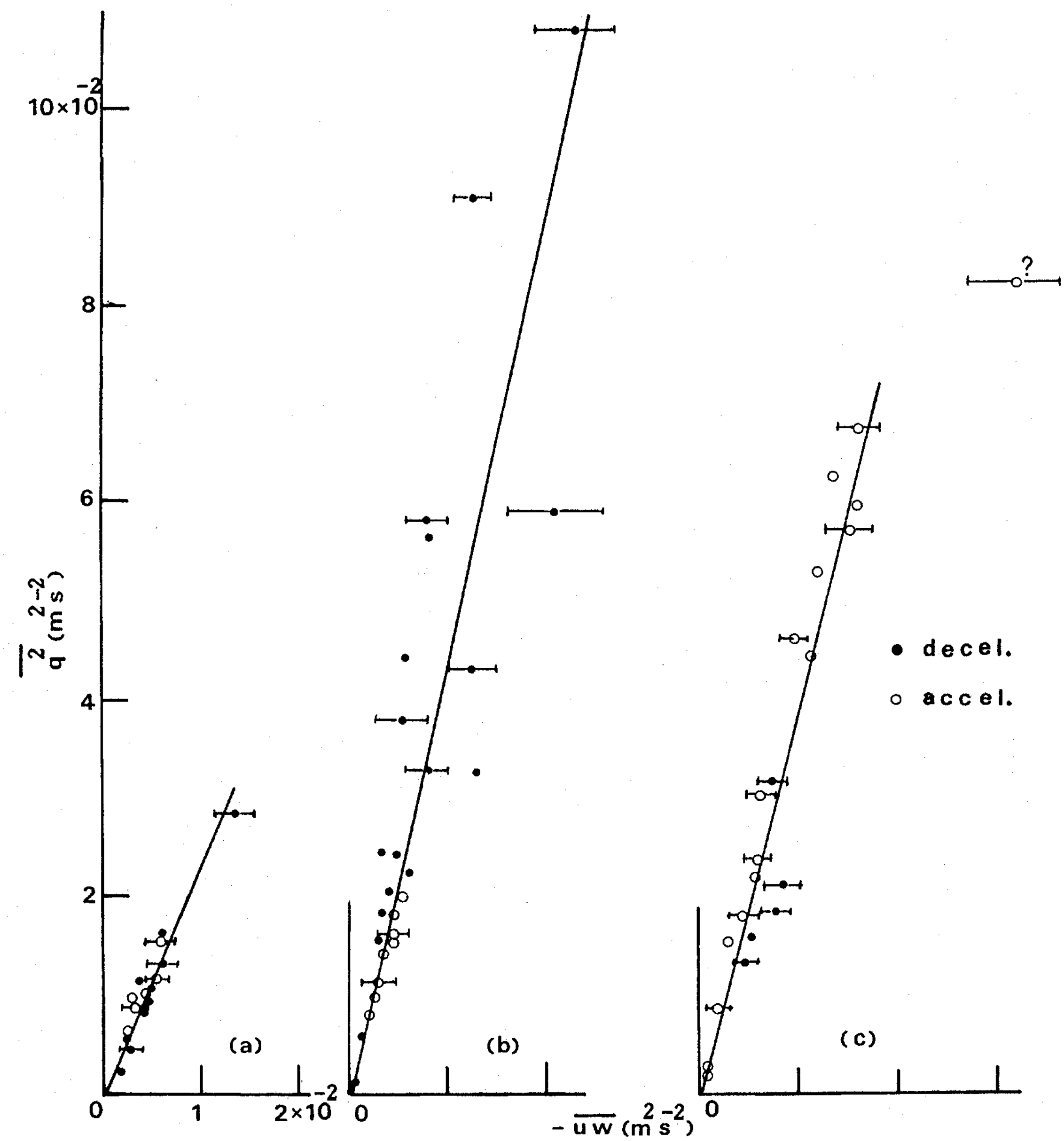


Fig 20 Variation of turbulent kinetic energy $\overline{q^2}$ with the Reynolds shear stress $(\overline{uw})^{1/2}$ at height z=0.35m, (a) ebb tide 7 June, (b) ebb tide 8 June, and (c) flood tide 8 June 1986.